2023 IEEE/ASME International Conference on Advanced Intelligent Mechatronics (AIM)
June 28-30, 2023. Seattle, Washington, USA

Error Diffusion based Feedforward Height Control for Inkjet 3D Printing

Yumeng Wu*, George Chiu†,
School of Mechanical Engineering
College of Engineering
Purdue University
West Lafayette, IN, 47907 USA
Email: *wu350@purdue.edu, †gchiu@purdue.edu

***Abstract*—Inkjet 3D printing is capable of building high-resolution components layer by layer with polymer-based materials that can also include functional components. Currently, most inkjet 3D printers are operated with prescribed layer structures to achieve a desired geometry and, in particular, a desired heigh profile. This often leads to discrepancy between target geometry and actual products. This article presents a framework to leverage halftoning processes in inkjet printing of images to inkjet 3D printing to improve geometric integrity and specifically a more precise height profile. By using the existing imaging pipeline, this framework requires no modification to current hardware. Halftone is a fundamental step in imaging pipeline for all digital printing systems. Error diffusion is one of the most common and widely used halftone algorithms. In this work, we will use two different error diffusion kernels, the 2×3 Floyd and Steinberg (FS) kernel and the 3×5 Jarvis, Judice and Ninke (JJN) kernel to demonstrate the feasibility and improve height profile control of an inkjet 3D printer using UV curable inks. The current implementation operates in a feedforward manner using a previously validated 2D height profile model to provide heigh estimation after the deposition of each layer. Two 3D geometry samples are printed using the proposed approach. Consistent RMS height profile errors and standard deviations from different samples demonstrated the effectiveness of the proposed approach to improve height profile tracking in inkjet 3D printing.**

***Index Terms*—Digital Printing, Additive Manufacturing, Process Modeling, Three-Dimensional Printing, Process Control, Image Processing**

I. Introduction

3D printing has emerged from a prototyping process and gained rapid growth in production in the last decade, achieving annual growth rate of 27.4%, reaching a market value of $12.8 billion [1]. Among different 3D printing methods, material jetting, or inkjet 3D printing, shares the same operation principles as inkjet image printing. Both processes dispense ink droplets through a nozzle. Instead of depositing droplets with color inks, inkjet 3D printers deposit inks made of photo-initiators [2]. Geometries are built by curing with ultraviolet (UV) light layer by layer [3]. Inkjet 3D printed components generally have higher resolution than other 3D printing methods and can be made of wider selection of materials [4]–[7]. Such advantages make it more suitable for biomedical and pharmaceutical applications [8], as well as fabricating microelectronics [9]–[11].

Geometric integrity is one of the key performance index to evaluate 3D printing quality. It is more important for functional printing, as the geometry can affect the efficacy or functionality in addition to geometric fit. Researchers have found that the drug delivery and sometimes the efficacy of the medicine can be affected by the drug shape [12]–[14]. The shape of microelectronics changes not only electrical properties, but also thermal and mechanical performance [15]. Process control is necessary to improve geometric integrity of the printed products. Spacial iterative learning control can reduce layer-to-layer error accumulation [16]. However, real-time height measurement is necessary, which can be overly expensive. Model predictive control is widely used for process control for its flexibility [17], but computation can be a potential impediment. Physics-guided reinforcement learning is also studied to improve print quality [18]. The high cost associated with collecting wide range of experimental data makes implementation costly. Besides the potential improvement of print quality with aforementioned process control methods, it is often difficult to utilize them for control of height profiles in real world implementation. These methods require modification of the existing system and extra training for the associated new workflow. Additionally, *in-situ* high resolution height measurement devices associated with these process control methods can be prohibitively expensive and require significant modification or redesign of existing systems.

On the other hand, improving height profile control of inkjet 3D printing can also rely on the similarities between inkjet 3D printing and its 2D counterpart. Image processing techniques have been studied extensively to improve printing quality leading to standardized workflow [19]–[21]. Continuous tone images are binarized for inkjet printers, as most inkjet printers cannot arbitrarily modulate its drop volume at a practical and useful rate. This process is called halftone [22]. Halftone techniques range from the straightforward constant thresholding, the slightly more complicated error diffusion [23], to the numerical-based direct binary search (DBS) [24]. More details on halftone are given in Sec. III-A. Apart from some

differences, height of a printed component can be interpreted as the tone of a monochrome image. Moreover, almost all halftone techniques are open-loop. As a result, adopting this path can avoid the high cost associated with in-situ high resolution real-time built height sensors.

In this work, a framework to leverage halftone algorithms as feedforward control candidates for inkjet 3D printing to improve geometric integrity is proposed. The framework interprets build height as a tone-like channel and utilizing a height profile propagation model [25] to quantify the impact of new drop on height profile. Thus, existing halftone process that have demonstrated their improvement on image printing quality can be adapted for inkjet 3D printing. The main advantages of this framework include relaxing the need for expensive real-time high-resolution height measurement and leveraging the hardware and firmware infrastructure used in digital imaging workflow to 3D printing. Error diffusion is chosen as an example to demonstrate the effectiveness of proposed approach through experiments.

The remaining of this article is organized in the following order. Section II states the problem and scope of this work. Section III introduces current halftone methods and our proposed framework. Section V is the experimental setup and validation with model-based error diffusion. Lastly, Section VI is the conclusion.

II. Height Profile Propagation Model

A previously validated height profile propagation model is used to predict the layer-to-layer height profile. The detailed work in [25] is briefly revisited here. The assumptions from the model include flat and non-porous substrate, no coalescence between adjacent uncured drops and consistent drop volume.

A pitch distance, d, between adjacent drops is predetermined based on th drop size, capability of motion controller and desired print quality. The $d \times d$ space centered at the desired print location is defined as a cell, which is the minimum controllable area. For a print area consisting of $\alpha \times \beta$ cells, the cell volume matrix of this print area after the k^{th} layer, $V[k]$, is denoted as a matrix of size $\alpha \times \beta$, where each element at row i column j, $v_{ij}[k]$, represents the percentage of volume of one drop in cell (i, j) after the k^{th} layer. Similarly, the cell area matrix of this print area after the k^{th} layer, $A[k]$, is denoted as a matrix of size $\alpha \times \beta$, where each element at row i column j, $a_{ij}[k]$, represents the percentage of area within the cell (i, j) covered by inks after the k^{th} layer. The cell height matrix of this print area after the k^{th} layer, $H[k]$, is denoted as a matrix of size $\alpha \times \beta$, where each element at row i column j, $h_{ij}[k]$, represents the average height cell (i, j) after the k^{th} layer. Since uncured inks flow due to uneven substrate, the cell height difference matrix after the k^{th} layer, denoted as $\tilde{H}[k]$, represents the average height difference to the 8 surrounding cells. It can be calculated by convolving $H[k]$ with a weighting matrix W, i.e.

$$\tilde{H}[k] = W * H[k], \tag{1}$$

where

$$W = \frac{1}{8}\begin{bmatrix} -1 & -1 & -1 \\ -1 & 8 & -1 \\ -1 & -1 & -1 \end{bmatrix}, \tag{2}$$

and $*$ denotes the convolution operation. The binary print map of the k^{th} layer, denoted as $U[k]$, where each element at row i column j uses 1 or 0 to represent whether a drop is printed or not, respectively.

The propagation model of the height profile is the result of two separate propagation models of cell volume and cell area. The volume matrix after the k^{th} layer is the summation of the volume matrix after the $(k-1)^{th}$ layer and the newly added volume due to the k^{th} layer. The propagation law can be written as

$$V[k] = V[k-1] + \Delta V[k], \tag{3}$$

where $\Delta V[k]$ is the newly added drop volume distribution due to the k^{th} layer. The newly added drop distribution $\Delta V[k]$ consists of two parts, a height difference dependent volume at the deposition cell and a constant distribution profile,

$$\Delta V[k] = m_v \tilde{H}[k-1] \odot U[k] + V_{std} * U[k], \tag{4}$$

where m_v is the empirically determined volume change coefficient, $U[k]$ is the print map of the k^{th} layer, $\tilde{H}[k-1]$ is the height difference matrix after the $(k-1)^{th}$ layer, V_{std} is the empirically determined volume distribution matrix, and $\odot$ denotes element-wise multiplication.

Following the same approach as volume propagation, the area matrix after the k^{th} layer is modeled as the summation of the area matrix after the $(k-1)^{th}$ layer and the newly added area due to the k^{th} layer. However, instead of keep expanding the occupied area in each cell, there is an upper limit to area coverage. The area occupied by the drop in each cell saturates to 1 when it is fully occupied. Thus, the propagation law can be written as

$$A[k] = \min(A[k-1] + \Delta A[k], [1]_{\alpha \times \beta}), \tag{5}$$

where $\Delta A[k]$ is the newly added area occupied by the drop in the cells due to the k^{th} layer. It is modeled as the addition of a constant profile in cells adjacent to the deposition location. Mathematically, it can be written as

$$\Delta A[k] = A_{std} * U[k]. \tag{6}$$

After both $V[k]$ and $A[k]$ are obtained, the height profile after the k^{th} layer, $H[k]$, can be calculated from

$$H[k] = c\frac{V[k]}{A[k]}, \tag{7}$$

where c is the scaling factor to convert percentage values to absolute height and the division is element-wise.

In summary, the height profile of the k^{th} layer can be estimated from the height of the $(k-1)^{th}$ layer and the binary print mask of the k^{th} layer $U[k]$ from Eqs. (1)–(7). The above model was experimentally validated to within 11% of the actual built height [25], which represents a 63% improvement from similar models in literature.

III. Leverage Image Processing Techniques for Inkjet 3D Printing

Inkjet 3D printing and color inkjet printing are very similar in their basic operations. While each channel in color printing, cyan, magenta, yellow and black (CMYK), prints only once at each location, inkjet 3D printing builds the product by depositing inks multiple times at the same location with solidification process between each layer. Thus, it is reasonable to treat height as a color. One notable difference between them is that the target intensity for an 8-bit color ranges between 0 and 255. However the target height for a 3D printed part can be any positive number. More importantly, the drop volume spills over to adjacent cells and the impact accumulates as more layers are printed.

Since the target color intensity is continuous while the inkjet printer can be operated only in binary mode, the target print must be processed and converted to a binary print map. Halftone is such process, which have been studied extensively in the past decades in imaging processing community. All halftone processes aim to make the perceived binary images to be as close as possible to the target continuous tone image. Given the similarities between inkjet 3D printing and its 2D sibling, adapting the knowledge of halftone processes for inkjet 3D printing would fast-track the improvement of inkjet 3D printing quality by leveraging existing hardware and software tools and image pipelines.

A. Halftone Image

A digital grayscale image only has one color/tone channel. Without loss of generosity, the remaining of the work uses grayscale images to represent digital images. An 8-bit tone channel uses an 8-bit integer, ranging from 0 to 255, to represent the intensity. Zero intensity represents there is no colorant is being added while full intensity represents the full colorant. Thus, 0 and 255 in a grayscale image represent white and black, respectively.

Most printers can deposit drop with constant volume, such that the only controllable input is whether or not a drop is deposited. Using binary representation, white is assigned to 0 and black is assigned to 1. As a result, all gray, ranging between 1 and 254, must be converted to 0 and 1 before sent to printer. The easiest method is rounding the intensity to the nearest integer, 0 or 255, before mapped to 0 and 1. However, images printed with this method are perceived by human eyes significantly different from the original ones. To address this issue, many researchers have studied extensively on halftone to map continuous tone images with binary images while making the perceived printed images closer to the original images.

Among other more complex halftone methods, error diffusion is widely used for its ease of implementation and simple computation. It has been the default halftone method for many printers. As suggested by its name, error diffusion diffuses the quantization error of the intensity to neighboring pixels, or more specifically, to pixels in the forward printing path. The error is calculated as the difference between the desired intensity and printed intensity. Besides white or black, there

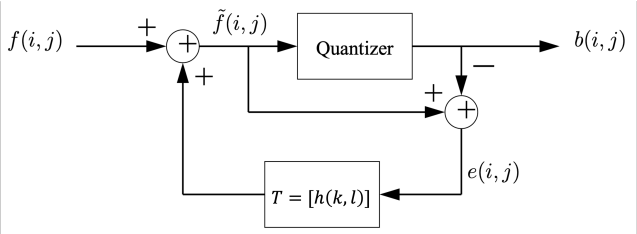

Fig. 1: The block diagram of error diffusion process on a pixel level [27].

are quantization errors when the desired intensity is gray when the only option is to print a full drop or skip the location. In general, each error is positive if the pixel is skipped or negative if it is deposited. This error is then spread towards the forward printing path following the predetermined error diffusion kernel. Floyd and Steinberg described a system with a 2×3 kernel to perform the error diffusion in 1976 [23]. Its kernel T_{FS} is described by

$$T_{FS} = [h(k,l)] = \frac{1}{16}\begin{bmatrix} - & \# & 7 \\ 3 & 5 & 1 \end{bmatrix}, \tag{8}$$

where $-$ represents previously processed pixels; # represents the current pixel and the values describe the percent of error to be spread to the corresponding pixel. Almost at the same time, Jarvis, Judice and Ninke of Bell Labs also published a similar method to improve the display quality, albeit with a 3×5 kernel [26]. Their kernel is described by

$$T_{JJN} = [h(k,l)] = \frac{1}{48}\begin{bmatrix} - & - & \# & 7 & 5 \\ 3 & 5 & 7 & 5 & 3 \\ 1 & 3 & 5 & 3 & 1 \end{bmatrix}. \tag{9}$$

Figure 1 illustrates the error diffusion process at the pixel level. $f(i,j)$ is the original intensity level at pixel location (i,j) before any processing, $h(k,l)$ is the corresponding error diffusion coefficient from the kernel. Eq. (8) or (9). $\tilde{f}(i,j)$ is the effective intensity level after processing. $b(i,j)$ is the quantized intensity level of $\tilde{f}(i,j)$, and $e(i,j)$ is the error to be spread towards forward pixels. Mathematically, the error diffusion process can be written as

$$\begin{aligned} b(i,j) &= \begin{cases} 1 & \text{if } \tilde{f}(i,j) > 0.5 \\ 0 & \text{otherwise} \end{cases} \\ e(i,j) &= \tilde{f}(i,j) - b(i,j) \\ \tilde{f}(i,j) &= f(i,j) + \sum_{k,l \in T} h(k,l) e(i-k, j-l) \end{aligned}, \tag{10}$$

where T is the error diffusion kernel and k,l is the location index of the kernel.

IV. Adapt Error Diffusion for Height Control

By treating height as tone intensity in monochrome inkjet printing, halftone techniques can be adopt for inkjet 3D printing described in this section. The proposed model-based error diffusion process is then experimentally validated on an inkjet 3D printing system.

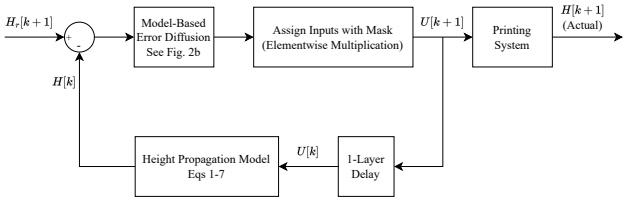

(a) The block diagram of the model-based error diffusion operated on one layer.

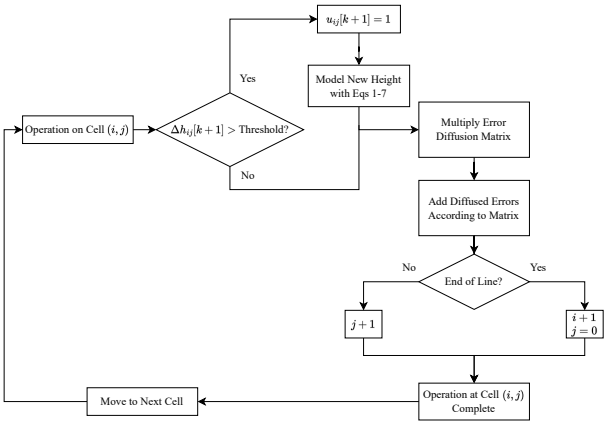

(b) The block diagram of the model-based error diffusion block.

Fig. 2: Block diagrams of the model-based error diffusion feedforward control on one layer and detailed view of the model-based error diffusion block.

The block diagram of the proposed model-based error diffusion process is shown in Fig. 2a. For the $(k+1)^{th}$ layer, its inputs include reference height of the $(k+1)^{th}$ layer, $H_r[k+1]$, and the estimated height of the k^{th} layer, $H[k]$, from the height propagation model. The maximum reference height in each cell is the desired cell height. The difference between the reference height and the feedback height is the input to the model-based error diffusion block, which is shown in Fig. 2b.

Within the model-based error diffusion block, each cell is processed with error diffusion before utilizing the height propagation model to estimate the height. This introduces the main difference from image halftone. When halftoning inks for inkjet 3D printing, spillover inks to adjacent cells contributes unevenly to the main cell and adjacent cells. Moreover, as more layers are printed, ink accumulate in each cell. As a result, its impact cannot be neglected. Image halftone neglects the impact of the spillover tone, since the spillover of inks share the same intensity and there is at most one layer of inks. Similar to image halftone, the print area is processed following the print direction or print path within each row before moving down to the next row. Such that error diffusion kernels can consistently diffuse errors to the forward print paths. Since the threshold of image halftone is 0.5, which is the half of the full tone intensity, the threshold of 3D printing halftone is

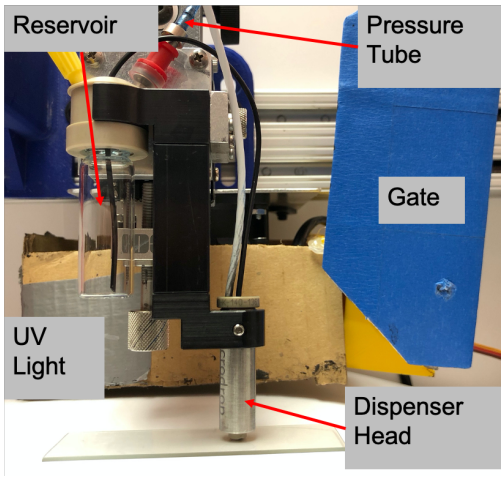

Fig. 3: The experimental setup. Gate closes when UV light is on to protect the dispenser head.

half of the mean layer height. If the error is greater then the threshold, a drop is deposited and the new height profile is adjusted. Height profile model presented in Sec. II is used to predict height change whenever there is a new drop. Either or not a drop is deposited, it is likely that the height is different from the reference height. Thus, height error is diffused to the forward path, same as image error diffusion. The output of the model-based error diffusion block is a binary print map of the layer.

The binary print map is then processed according to a print mask. This mask is predetermined to fit the printing system and also ensuring non-coalescence between drops. The resulting binary print map, $U[k+1]$, is sent to the printing system. The height profile after the $(k+1)^{th}$ layer is obtained for the next layer. This process repeats until the desired height is achieved.

V. Experimental Setup and Validation

A. Experimental Setup

The dispensing and curing part of the experimental system is shown in Fig. 3. The pressure tube connects to the back-pressure controller maintaining adequate miniscule at nozzle tip. The reservoir is always covered to prevent the ink inside from gradually curing due to ambient UV light. The gate closes when the UV light is on, to protect the dispenser head from clogging. The dispenser head is capable of heating the 70 μm diameter tip up to 100 $^{\circ}C$. The measurements are carried on a Zeta optical profilometer with a 50x objective lens and a 0.35x coupler. The z-axis resolution of the profilometer is 0.04 μm and the pixel area (a_c) is 0.49 m^2 at this setting. More details about the experimental system can be found in [25].

The printing control program is capable of adjusting print map between consecutive layers according to the control effort. In addition, while the current system does not connect to a real-time height sensing system, both hardware and software

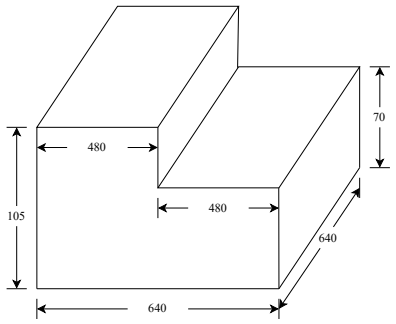

(a) Schematics of the desired bi-level print sample (in μm).

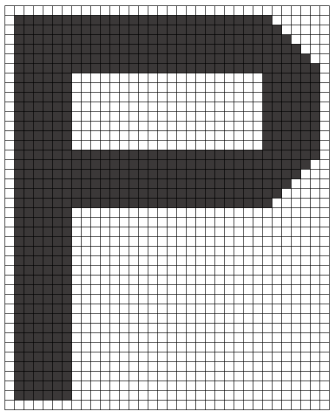

(b) The 6-pixel wide bit map of the character *P* to be printed. The nominal printing layer is 10 for the estimated height of 70 μm.

Fig. 4: Target prints used in experimental validation.

TABLE I: Compare error diffusion with uncontrolled print on the bi-level pattern
LH: Lower Half HH: Higher Half

	Uncontrolled	FS Kernel	JJN Kernel
LH Target Height (μm)	70	70	70
LH Mean Height (μm)	98.1	64.2	77.5
LH STD (μm)	24.5	13.7	12.6
HH Target Height (μm)	105	105	105
HH Mean Height (μm)	141.3	107.8	108.4
HH STD (μm)	27.1	20.96	19.98

are ready to interface if one is available. Currently, the system uses layer-to-layer height profile propagation model to predict the height profile.

B. Experimental Validation of Model-Based feedforward Error Diffusion for Inkjet 3D Printing

Two different patterns are printed for experimental validation. The controlled prints are made with both Floyd and Steinberg (FS) kernel and Jarvis, Judice and Ninke (JJN) kernel, and are compared with uncontrolled prints. The mean final height error and the associated standard deviation are used measure smoothness.

A 8×8 square bi-level pattern is used to determine the performance of flat surfaces. A larger *P* pattern to evaluate larger print area. All uncontrolled prints are based on a 7 μm mean layer height.

The target heights of the lower and the higher half of the bi-level patter are 70 μm and 105 μm, respectively. They translate to 10 and 15 nominal layers for the uncontrolled prints, respectively. A schematic is shown in Fig. 4a. The experimental results of the bi-level prints are summarized in Table I. Their contour plots are shown in Fig. 5, where from left to right are bi-level prints without control, controlled with model-based error diffusion using FS kernel and JJN kernel. Both prints with model-based error diffusion method outperform uncontrolled prints in terms of standard deviation. With larger error diffusion kernel, JJN kernel tends to achieve lower standard deviation than the smaller FS kernel consistently. As for the height profile, both prints with model-based error diffusion method achieve height close to the target height of 105 μm in the higher section. However, the print with FS kernel is lower than the desired 70 μm, while the print with JJN kernel is higher than the target height. In comparison, the uncontrolled print is much higher than the target height in both high and low section. The standard deviation from uncontrolled print is almost twice as much as that from controlled prints.

In addition to the bi-level components, a larger character *P* was printed. The print map is shown in Fig. 4b, where each line is 6-pixel wide and the total span is 40×32 pixels, or 4 $mm \times 3.2$ mm. The target height is 70 μm, which translates to 10 nominal layers for uncontrolled prints and the pitch distance is 100 μm. The experimental results of the bi-level prints are summarized in Table II. Their contour plots are shown in Fig. 6, where from left to right are bi-level prints without control, controlled with model-based error diffusion using FS kernel and JJN kernel. To improve readability, each grid represents 4-cell wide. Thus, each grid is 400 μm apart from each other. While the difference among different methods is not as significant as that on bi-level prints, both model-based halftone controlled prints outperform the uncontrolled one, in terms of closer to target mean height and smoother top surface. More specifically, the mean height error to the target 70 μm of the uncontrolled print is close to the mean layer height, which is the minimum controllable interval, while that error of both controlled prints are within half of the mean layer height. The standard deviation of the two controlled prints are 20% smaller than the uncontrolled print. Within the two controlled prints, using JJN kernel lead to slightly smoother top surface than the one with FS kernel, similar to the bi-level prints.

VI. Conclusion

In this paper, a model-based feedforward height control using error diffusion is proposed. It uses a previously validated height propagation model to predict built height of 3D printed pattern. A feedforward control algorithm is developed to generate print mask for subsequent layers to achieve improved height control. Experimental results validated the effectiveness

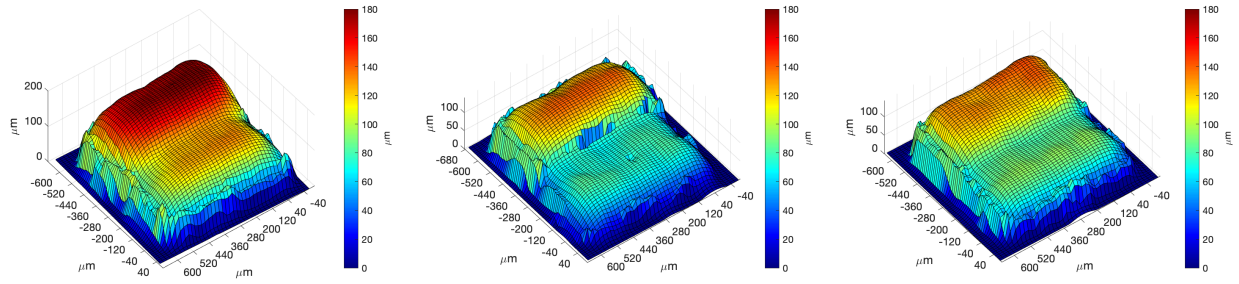

(a) Uncontrolled (b) FS kernel (c) JJN kernel

Fig. 5: From left to right are the experimental results of bi-level prints without any control, controlled with model-based feedforward error diffusion using FS kernel and JJN kernel. The analysis is shown in Tab. I

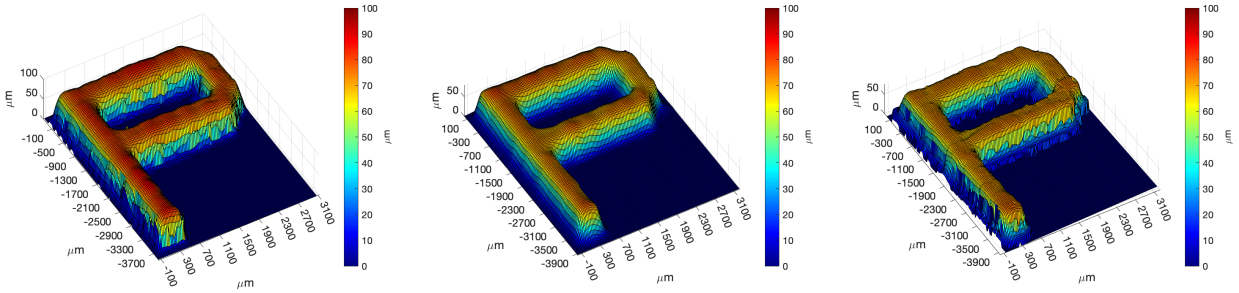

(a) Uncontrolled (b) FS kernel (c) JJN kernel

Fig. 6: From left to right are the experimental results of bi-level prints without any control, controlled with model-based feedforward error diffusion using FS kernel and JJN kernel. The analysis is shown in Tab. II

TABLE II: Compare error diffusion with uncontrolled print on the P pattern

	Uncontrolled	FS kernel	JJN kernel
Target Height μm	70	70	70
Mean Height (μm)	76.82	71.71	68.64
STD (μm)	15.99	12.45	11.01

of the proposed approach to improve built height control as well as improve overall surface smoothness. With real-time height feedback, the proposed approach can be easily converted to perform closed-loop height control for inkjet 3D printing. Although error diffusion is used in this study, other halftone techniques can also be adopted.

REFERENCES

[1] T. Wohlers, *Wohlers Report 2021, 3D Printing and Additive Manufacturing State of the Industry*. Wohlers Associates, Inc., 2021.

[2] S. Magdassi, *The chemistry of inkjet inks*. World scientific, 2009.

[3] K. Barton, D. Bristow, D. Hoelzle, and S. Mishra, "Mechatronics advances for the next generation of am process control," *Mechatronics*, vol. 64, p. 102281, 2019.

[4] S. Gantenbein, K. Masania, W. Woigk, J. P. Sesseg, T. A. Tervoort, and A. R. Studart, "Three-dimensional printing of hierarchical liquid-crystal-polymer structures," *Nature*, vol. 561, no. 7722, pp. 226–230, 2018.

[5] Y. Guo, H. S. Patanwala, B. Bognet, and A. W. K. Ma, "Inkjet and inkjet-based 3d printing: connecting fluid properties and printing performance," *D printing*, vol. 23, no. 3, p. 15, 2017.

[6] Q. Cheng, Y. Zheng, T. Wang, D. Sun, and R. Lin, "Yellow resistant photosensitive resin for digital light processing 3d printing," *Journal of Applied Polymer Science*, vol. 137, no. 7, p. 48369, 2 2020.

[7] Y. He, R. Foralosso, G. F. Trindade, A. Ilchev, L. Ruiz-Cantu, E. A. Clark, S. Khaled, R. J. M. Hague, C. J. Tuck, F. R. A. J. Rose, and et al., "A reactive prodrug ink formulation strategy for inkjet 3d printing of controlled release dosage forms and implants," *Advanced Therapeutics*, p. 1900187, 2 2020.

[8] T. Simpson, C. Williams, and M. Hripko, "Preparing industry for additive manufacturing and its applications: Summary & recommendations from a national science foundation workshop," *Additive Manufacturing*, vol. 13, 09 2016.

[9] S.-Y. Wu, C. Yang, W. Hsu, and L. Lin, "3d-printed microelectronics for integrated circuitry and passive wireless sensors," *Microsystems & Nanoengineering*, vol. 1, no. 1, pp. 1–9, 2015.

[10] T. Tilford, S. Stoyanov, J. Braun, J. C. Janhsen, M. K. Patel, and C. Bailey, "Comparative reliability of inkjet-printed electronics packaging," *IEEE Transactions on Components, Packaging and Manufacturing Technology*, vol. 11, no. 2, pp. 351–362, 2021.

[11] K. Y. Mitra, A. Willert, R. Chandru, R. R. Baumann, and R. Zichner, "Inkjet printing of bioresorbable materials for manufacturing transient microelectronic devices," *Advanced Engineering Materials*, vol. 22, no. 12, p. 2000547, 2020.

[12] O. Blazhenkova and K. Dogerlioglu-Demir, "The shape of the pill: Perceived effects, evoked bodily sensations and emotions," *PLOS ONE*, vol. 15, no. 9, p. e0238378, 9 2020.

[13] S. Crunkhorn, "Star-shaped pill sustains drug release," *Nature Reviews Drug Discovery*, vol. 16, no. 1, p. 16–16, 1 2017.

[14] A. Goyanes, P. Robles Martinez, A. Buanz, A. W. Basit, and S. Ga-

isford, "Effect of geometry on drug release from 3d printed tablets," *International Journal of Pharmaceutics*, vol. 494, no. 2, p. 657–663, 10 2015.
[15] R. Dadsetani, G. Sheikhzade, M. Goodarzi, A. Zeeshan, R. Ellahi, and M. R. Safaei, "Thermal and mechanical design of tangential hybrid microchannel and high-conductivity inserts for cooling of disk-shaped electronic components," *Journal of Thermal Analysis and Calorimetry*, vol. 143, no. 3, pp. 2125–2133, 2021.
[16] L. Aarnoudse, C. Pannier, Z. Afkhami, T. Oomen, and K. Barton, "Multi-layer spatial iterative learning control for micro-additive manufacturing," *IFAC-PapersOnLine*, vol. 52, no. 15, pp. 97–102, 2019.
[17] Y. Guo, J. Peters, T. Oomen, and S. Mishra, "Distributed model predictive control for ink-jet 3D printing," in *2017 IEEE International Conference on Advanced Intelligent Mechatronics (AIM)*. IEEE, 7 2017, pp. 436–441.
[18] M. F. Alam, M. Shtein, K. Barton, and D. J. Hoelzle, "A physics-guided reinforcement learning framework for an autonomous manufacturing system with expensive data," in *2021 American Control Conference (ACC)*. IEEE, 2021, pp. 484–490.
[19] D. L. Lau and G. R. Arce, *Modern digital halftoning*. CRC Press, 2018.
[20] M. P. Ekstrom, *Digital image processing techniques*. Academic Press, 2012, vol. 2.
[21] B. Chitradevi and P. Srimathi, "An overview on image processing techniques," *International Journal of Innovative Research in Computer and Communication Engineering*, vol. 2, no. 11, pp. 6466–6472, 2014.
[22] J. M. White and G. D. Rohrer, "Image thresholding for optical character recognition and other applications requiring character image extraction," *IBM Journal of research and development*, vol. 27, no. 4, pp. 400–411, 1983.
[23] R. W. Floyd and L. Steinberg, "An adaptive algorithm for spatial grayscale," *Proceedings of the Society of Information Display*, vol. 17, no. 2, pp. 75–77, 1976.
[24] M. Analoui and J. P. Allebach, "Model-based halftoning using direct binary search," in *Human Vision, Visual Processing, and Digital Display III*, vol. 1666. International Society for Optics and Photonics, 1992, pp. 96–108.
[25] Y. Wu and G. Chiu, "An improved model of height profile for drop-on-demand print of ultraviolet curable ink," *ASME Letters in Dynamic Systems and Control*, vol. 1, no. 3, p. 031010, 2021.
[26] J. Jarvis, C. Judice, and W. Ninke, "A survey of techniques for the display of continuous tone pictures on bilevel displays," *Computer Graphics and Image Processing*, vol. 5, no. 1, pp. 13–40, 1976.
[27] C. A. Bouman, "Digital image processing," 2021.